Relating Eulerian and Lagrangian Statistics for the Turbulent Dispersion in the Atmospheric Convective Boundary Layer

ALESSANDRO DOSIO, JORDI VILÁ-GUERAU DE ARELLANO, AND ALBERT A. M. HOLTSLAG

Meteorology and Air Quality Section, Wageningen University, Wageningen, Netherlands

PETER J. H. BUILTJES

TNO-MEP, Apeldoorn, Netherlands

(Manuscript received 9 March 2004, in final form 6 August 2004)

ABSTRACT

Eulerian and Lagrangian statistics in the atmospheric convective boundary layer (CBL) are studied by means of large eddy simulation (LES). Spectra analysis is performed in both the Eulerian and Lagrangian frameworks, autocorrelations are calculated, and the integral length and time scales are derived. Eulerian statistics are calculated by means of spatial and temporal analysis in order to derive characteristic length and time scales. Taylor's hypothesis of frozen turbulence is investigated, and it is found to be satisfied in the simulated flow.

Lagrangian statistics are derived by tracking the trajectories of numerous particles released at different heights in the turbulent flow. The relationship between Lagrangian properties (autocorrelation functions) and dispersion characteristics (particles' displacement) is studied through Taylor's diffusion relationship, with special emphasis on the difference between horizontal and vertical motion. Results show that for the horizontal motion, Taylor's relationship is satisfied. The vertical motion, however, is influenced by the inhomogeneity of the flow and limited by the ground and the capping inversion at the top of the CBL. The Lagrangian autocorrelation function, therefore, does not have an exponential shape, and consequently, the integral time scale is zero. If distinction is made between free and bounded motion, a better agreement between Taylor's relationship and the particles' vertical displacement is found.

Relationships between Eulerian and Lagrangian frameworks are analyzed by calculating the ratio β between Lagrangian and Eulerian time scales. Results show that the integral time scales are mainly constant with height for $z/z_i < 0.7$. In the upper part of the CBL, the capping inversion transforms vertical motion into horizontal motion. As a result, the horizontal time scale increases with height, whereas the vertical one is reduced. Current parameterizations for the ratio between the Eulerian and Lagrangian time scales have been tested against the LES results showing satisfactory agreement at heights $z/z_i < 0.7$.

1. Introduction

Atmospheric dispersion is a topic of great importance, especially in relation to pollutant transport. Two different approaches, known as the *Eulerian* and the *Lagrangian* frameworks, are used to describe this process.

In the Eulerian framework, statistical properties are calculated in a fixed reference frame. This approach is most commonly used in field experiments, with surface or aircraft platforms (Briggs 1993; Lenschow and Stankov 1986), as well as in laboratory experiments (Willis and Deardorff 1976, 1981; Weil et al. 2002) or Eulerian numerical models (Lamb 1978; Henn and Sykes 1992; Mason 1992). In the Lagrangian framework, the statistical properties are calculated in a reference frame that moves with the flow. This is the most natural approach for theoretical investigation of turbulent dispersion, as in the works by Taylor (1921) and Batchelor (1949), who established seminal theoretical relationships between dispersion parameters and turbulent characteristics in flows characterized by homogeneous turbulence. These relationships have been widely applied in studies of atmospheric dispersion in the atmospheric boundary layer (ABL). Turbulence in the atmospheric convective boundary layer (CBL), however, is vertically inhomogeneous, and the flow is generally characterized by large downdrafts of cold air surrounded by narrow strong updrafts of warm air. As a result, the vertical velocity is positively skewed, and the turbulent transport is asymmetric (Wyngaard and Weil 1991). Another relevant aspect in atmospheric dis-

Corresponding author address: Dr. A. Dosio, Meteorology and Air Quality Section, Wageningen University, 6701 AP Wageningen, Netherlands.
E-mail: alessandro.dosio@wur.nl

persion is that the vertical transport is confined between the surface and the inversion at the top of the CBL.

Previous theoretical analysis has been applied to inhomogeneous flows, in particular in the works by de Baas et al. (1986), Georgopoulos and Seinfeld (1988), and Degrazia et al. (1998), who related dispersion parameters and Lagrangian properties (like the integral time scale) to spectral characteristics of the atmospheric CBL.

Experimental measures of Lagrangian statistics in the CBL are very difficult to obtain. Experiments with grid-generated isotropic turbulence (e.g., Sato and Yamamoto 1987; Voth et al. 1998; Ott and Mann 2000) are only partly representative of the turbulent transport in the atmosphere. Measurements of Lagrangian statistics in the atmosphere require the use of neutrally buoyant balloons (Gifford 1955; Angell 1964; Hanna 1981). As pointed out by Hanna (1981), due to the complicated experimental setting required in order to trace the balloon trajectory, the small number of balloons used, and the short sampling time (which rarely exceeds 30 min), experimental estimates of the Lagrangian time scale have solely an accuracy of about 50%.

Another alternative method to calculate Lagrangian statistics is by means of numerical simulations; that is, the trajectories of particles released in a numerically generated turbulent flow are tracked in space and time. The most accurate approach is direct numerical simulation (DNS) by which the governing equations of the turbulent motion are directly solved numerically. Due to the high number of degrees of freedom needed to solve all the scales of motion of turbulence, Yeung and Pope (1989) and Squires and Eaton (1991) investigated Lagrangian properties of isotropic turbulence only at low Reynolds numbers, therefore making it difficult to extrapolate the results to atmospheric applications.

Since Lagrangian statistics are strongly influenced by the large scales of motion (Wang et al. 1995), a more suitable approach for studying Lagrangian statistics in the ABL is by large eddy simulation (LES). By simulating the atmospheric flow with LES, the largest energy-containing scales of motion are solved directly, and only the effect of the smallest (subgrid) scales are parameterized (e.g., Nieuwstadt et al. 1991). To our knowledge, only very few studies have investigated Lagrangian statistics using LES: Wang et al. (1995) studied the ratio of the Lagrangian to the Eulerian time scales and the particles' mean-square dispersion in a simulated turbulent channel flow, a highly idealized approximation of the neutral ABL. The Lagrangian statistics were only calculated for two different values of the Reynolds number (Re = 3200 and Re = 21 900) and only at a few selected levels within the boundary layer (BL). Uliasz and Sorbjan (1999) calculated vertical profiles of Lagrangian time scales in the CBL, but neither further investigation on other turbulence properties (such as the energy spectra) nor direct application to dispersion characteristics was made.

In our study, an LES is used to calculate Eulerian and Lagrangian statistics in the atmospheric CBL. In contrast to field measurements, the numerical simulation represents a very controlled experiment because the flow characteristics are prescribed through initial and boundary conditions. In addition, the use of a large numerical domain and a long integration time allow us to obtain reliable statistics in both space and time.

Three main research issues are addressed in this study: First, the turbulent characteristics of the flow are studied in the Eulerian framework by analyzing the energy spectra and velocity autocorrelations. Spatial and temporal analysis are carried out in order to derive length and time scales. These integral scales are usually related by Taylor's hypothesis of frozen turbulence. The LES results allow us to investigate the validity of Taylor's hypothesis in our numerically simulated CBL.

Second, Lagrangian statistics are calculated, and the relationship between flow properties (autocorrelations) and dispersion characteristics (particles' displacements) is discussed through Taylor's analysis of turbulent dispersion (Taylor 1921).

Finally, the relationship between Eulerian and Lagrangian frameworks is studied by calculating the ratio β between the Lagrangian and Eulerian time scales. This is relevant for improving the description of turbulent dispersion in the CBL and for relating theoretical approaches to experimental studies. Currently used parameterizations derived either in previous field atmospheric experiments (Hanna 1981) or through theoretical analysis based on analytical spectra (Degrazia et al. 1998) are validated against the LES results.

The outline of the paper is as follows: The theoretical background of the research is provided in section 2; in section 3, the numerical experimental setup is described, and definitions of the calculated variables are given. The LES results for the Eulerian and Lagrangian statistics are then presented and discussed in sections 4 and 5, respectively. In section 6, the application of these statistics to atmospheric dispersion is examined. Finally, in section 7, the relationship between the two frameworks is studied. The range of validity of existing parameterizations for the value of the Lagrangian time and the ratio between Lagrangian and Eulerian time scales are also compared with the LES results.

2. Theoretical background

Dispersion in the atmosphere is related to the displacement of particles from one another. Assuming an ensemble of particles moving in the turbulent flow, the displacement in the jth direction, at a time t after the release, is defined as

$$\overline{x_j'^2}(t) = \overline{[x_j^i(t) - \overline{x_j^i(t)}]^2}, \tag{1}$$

where $x_j^i(t)$ is the position of the ith particle, and the overbar represents the average over all the particles.

Following the classical analysis of Taylor (1921), this displacement is expressed as a function of the properties of the turbulent flow according to

$$\overline{x_j'^2}(t) = 2\sigma_j^2 \int_0^t \int_0^{t'} R_j^{\mathrm{L}}(\tau) d\tau \, dt', \tag{2}$$

where σ_j is the (square root of the) velocity variance, and $R_j^{\mathrm{L}}(\tau)$ is the Lagrangian autocorrelation function, defined as

$$R_j^{\mathrm{L}}(\tau) = \frac{\overline{u_j'(t) u_j'(t+\tau)}}{\sigma_j^2}. \tag{3}$$

Here, $u_j'(t) = u_j^i(t) - \overline{u_j^i(t)}$ is the velocity fluctuation of the ith particle at time t, and τ is the time lag.

Relationship (2) has two analytical limits for short and large times, respectively,

$$\overline{x_j'^2}(t) = \sigma_j^2 t^2 \qquad t \ll T_j^{\mathrm{L}} \quad \text{and} \tag{4}$$

$$\overline{x_j'^2}(t) = 2\sigma_j^2 T_j^{\mathrm{L}} t \quad t \gg T_j^{\mathrm{L}}, \tag{5}$$

where the Lagrangian (integral) time scale T_j^{L} is defined as (e.g., Hinze 1975)

$$T_j^{\mathrm{L}} = \int_0^{\infty} R_j^{\mathrm{L}}(\tau) d\tau. \tag{6}$$

There is a large uncertainty in the value of the Lagrangian time scale and its dependence to other variables of the ABL. For instance, values reported in literature vary from $T_{v,w}^{\mathrm{L}} \sim 80$ s (Hanna 1981) to $T_v^{\mathrm{L}} \sim 10\,000$ s (Gifford 1987). Theoretical analysis by Degrazia et al. (1998) relates the Lagrangian time scale to flow characteristics (for details see section 7):

$$T_j^{\mathrm{L}} \sim C \frac{z_i}{\sigma_j}, \tag{7}$$

where the value of the constant ($C \sim 0.17$) is in agreement with the experimental results by Hanna (1981) in the middle of the CBL.

Lagrangian statistics are seldom measured experimentally in the CBL, and T_j^{L} is normally inferred from Eulerian statistics using the following relationship:

$$T_j^{\mathrm{L}} = \beta_j T_j^{\mathrm{E}}, \tag{8}$$

where T_j^{E} is the Eulerian integral time scale, and β_j is the ratio of the Lagrangian to Eulerian time scales. Atmospheric measurements of β_j usually range between 3 and 4 (Gifford 1955; Angell 1964), whereas Hanna (1981) found a value of $\beta_j = 1.6$.

The value of β_j is dependent on the turbulence intensity $i = \sigma_j/U$ [where $U = U(z)$ is the mean wind speed] by the relationship,

$$\beta_j = \frac{C}{i} = C \frac{U}{\sigma_j}, \tag{9}$$

where the value of the constant C ranges in the literature from 0.35 to 0.8 (see, e.g., Wang et al. 1995), with a theoretical value of 0.44 (Wandel and Kofoed-Hansen 1962) and an experimentally measured value of 0.7 (Hanna 1981). Numerical simulations by Wang et al. (1995) led to $C = 0.6$.

LES allows us to calculate Eulerian and Lagrangian statistics for an atmospheric CBL within the same numerical experiment. From the LES results, the autocorrelation function (3) in calculated in both Eulerian and Lagrangian frameworks, and the integral scale (6) is derived. From the computed particle trajectories, dispersion statistics (1) are calculated and related to the turbulent characteristics of the flow through (2). By so doing, we investigate the influence of the inhomogeneity of the flow and the CBL boundaries on atmospheric dispersion.

Finally, the values of the Lagrangian time scale and the ratio β_j (8) are compared with experimental measurements and previously proposed parameterizations [Eqs. (7) and (9)].

3. Description of the numerical experiment

The LES code used here was the parallelized version of the one described by Cuijpers and Duynkerke (1993) and Siebesma and Cuijpers (1995), in which a set of filtered prognostic equations for the dynamic variables (wind velocity, potential temperature, and turbulent kinetic energy) was solved on a staggered numerical grid. The space and time integrations were computed with a kappa (Vreugdenhil and Koren 1993) and leapfrog numerical schemes, respectively.

The numerical domain covered an area of 10.240×10.240 km^2. A horizontal grid length of 40 m was used (256 grid points in each horizontal direction). A nonuniform grid of 96 points was used in the vertical direction, with the vertical grid resolution varying from 5 m near the surface to 15 m above the surface layer.

The subgrid fluxes were closed by relating them to the gradient of the solved variable by means of an exchange coefficient, which depended on the subgrid turbulent kinetic energy, and a length scale, which was related to the grid size. By so doing, the grid anisotropy was to a certain extent implicitly taken into account by the subgrid closure. The aspect ratio, that is, the ratio of the horizontal domain dimension to the CBL height z_i, was around 10 (with $z_i \sim 940$ m). Lateral periodic boundary conditions were imposed for all the variables. A time step of 0.25 s was used.

At the top of the CBL, an inversion strength of $\Delta\theta = 5$ K was imposed, which strongly limited the vertical motion of the flow in the entrainment zone. As shown by Moeng and Rotunno (1990), the turbulent flow near the top of the CBL is strongly influenced by the capping inversion; the updrafts convert their kinetic energy into that of horizontal motion. Moreover, in this region,

there are fewer updrafts than in the middle of the CBL. As a result, the skewness of the vertical velocity increases. The change of the turbulence structure due to the strong inversion has a large impact on the particles' vertical motion, as will be discussed later.

A geostrophic wind of 5 m s^{-1} aligned in the x direction and a heat flux of 0.156 K m s^{-1} were imposed as constant forcing, and the simulation was run for an initialization period of 2 h [i.e., the period of CBL development needed to ensure that a (quasi) stationary state is reached]. After this period, the gradients of the mean variables were independent of time, and the turbulent kinetic energy had become constant. The average values of the convective velocity scale w_* was 1.7 m s^{-1} and the shear/buoyancy ratio u_*/w_* was equal to 0.21 (where u_* is the friction velocity). The value of the stability parameter $-z_i/L$ was ~40. According to the classification used by Holtslag and Nieuwstadt (1986), this simulated flow is mainly driven by convective turbulence.

a. Lagrangian particle model

After the initialization period, 1024 particles were released on a regular horizontal grid at 50 different levels (from $z = 100$ m to $z = 850$ m), that is, a total of 51 200 particles. The horizontal distance (x and y direction) between the initial position of each particle was 320 m, in order to assure statistical independence. The position and velocity of each particle were recorded every 5 s for the following 5120 s. Here, it is important to point out that the Lagrangian statistics (autocorrelations and integral scales) are mainly dependent on the contribution of the largest scale of motion. For example, the integral scale is directly related to the peak of the energy spectra (Hanna 1981); therefore, a long sampling time is required to completely solve the most relevant scales of motion. Besides, tracking the particle using shorter time steps does not improve the results at smaller scales. In fact, since the horizontal grid size is 40 m and the mean wind speed is 5 m s^{-1}, each particle remains in a numerical grid cell for an average time of 8 s. Scales of motion smaller than the grid size are therefore filtered out by the LES. A test performed by tracking the particle every second did not show significant differences in the particle trajectories and velocities.

The position in the direction j of the ith particle was calculated according to

$$x_j^i(t + \Delta t) = x_j^i(t) + u_j^i(t)\Delta t, \tag{10}$$

where Δt is the time step, and $u_j^i(t)$ is the velocity of the particle calculated by linearly interpolating the values of the resolved (Eulerian) velocity at the eight closest grid points. As pointed out by Weil et al. (2004), for a more realistic calculation of the particle's position, the subgrid component of the velocity $u_j^{i\prime}$ should be included in (10). The value of $u_j^{i\prime}$, which is not directly available from the LES, could be computed by solving the Langevin equation using a Markov chain process, as suggested by Gopalakrishnan and Avissar (2000) or by a simple random walk scheme (Uliasz and Sorbjan 1999). A different approach was used by Mason (1992), who added a random vertical displacement to the motion of the particles close to the surface. Finally, Weil et al. (2004) used an adaptation of Thomson's (1987) Lagrangian Stochastic Modelin which $u_j^{i\prime}$ is specified by a Gaussian probability density function (PDF) based on the subgrid stress tensor.

The subgrid velocity is particularly relevant in regions characterized by strong gradients, such as near the surface, and may lead to errors in the calculation of ground concentration (Weil et al. 2004). In our study, particles are released between $z/z_i = 0.12$ and $z/z_i = 0.9$, where the flow is characterized by constant profiles of wind and potential temperature.

Moreover, as discussed earlier, a quantity such as the Lagrangian time scale is dependent on the velocity contributions of the lower frequencies only, and therefore the velocity subgrid scales are not very relevant. This is corroborated by previous studies by Wang et al. (1995) and by Gopalakrishnan and Avissar (2000), who found no significative difference in the results if the velocity subgrid component was taken into account. Also, a simulation run with a finer grid ($10 \times 10 \times 10$ m) did not show differences in the results at large scales, as discussed below. The subgrid velocity $u_j^{i\prime}$ was therefore not included in our calculations.

A similar argument is used with respect to the choice of the interpolation method to calculate the Lagrangian velocities $u_j^i(t)$ from the Eulerian (resolved) ones [(10)]. Although the linear interpolation is used by many authors (Uliasz and Sorbjan 1999; Mason 1992), it is inadequate, as it may introduce numerical noise when the particle cross the grid-line boundaries (Yeung 2002). Nevertheless, the error (imprecision) associated with this process is only relevant at the smallest scales (i.e., scales equal or smaller than the numerical grid). Since the Lagrangian statistics (both autocorrelations and integral scales) are associated with the largest scale of motion, which are explicitly solved by the LES, we are confident that for the atmospheric flow the results are rather independent of the interpolation scheme used.

b. Definition of statistical variables

Autocorrelation functions and integral scales are calculated from the LES results in both the Eulerian and Lagrangian frameworks.

In the Eulerian framework, both temporal (E_t) and spatial (E_s) analyses are performed. Temporal analysis is the calculation of statistics from time series collected at fixed positions. Spatial analysis is the calculation of statistics from data collected at different locations at fixed time (or averaged over a certain time).

In the Lagrangian framework (L), statistics are cal-

culated from the particle velocities calculated by the LES according to (10). These different approaches are illustrated schematically in Fig. 1. The theoretical definition of the autocorrelation functions in the different frameworks is reported in the appendix. From the autocorrelation, the integral length scales (λ) and time scales (T) are derived in both Eulerian and Lagrangian frameworks. There are two drawbacks in the determination of the integral scales according to (6). First, if the sampling time is limited, the autocorrelation may not approach zero, a problem encountered by Hanna (1981) in his Lagrangian field experiment. Second, if the autocorrelation shows oscillations around zero (e.g., Deardorff and Willis 1985), the value of the integral scale calculated by (6) is zero. This is the case for wavelike signals, as shown by Csanady (1973).

The autocorrelation function for a pure stochastic motion has an exponential shape, that is, $R(\tau) = \exp(-\tau/T)$, where T is the integral scale (Csanady 1973). In this case, the integral scale calculated by (6) is equal to the time T_e required for the autocorrelation to drop to $1/e$. Therefore, the measurement of T_e is the method commonly used in the majority of the studies related to atmospheric flows (Hanna 1981; Wang et al. 1995; Deardorff and Willis 1985; Mason 1989). As will be discussed later, in the atmospheric CBL, the shape of the autocorrelation for the vertical velocity may differ from that of a simple exponential, and therefore the use of T_e as the definition of integral scale is not appropriate.

In our study, the integral scales are defined according to (Lenschow and Stankov 1986)

$$\begin{cases} T = \max\left[\int_0^t R(\tau)d\tau\right] \\ \lambda = \max\left[\int_0^r R(r')dr'\right] \end{cases}. \tag{11}$$

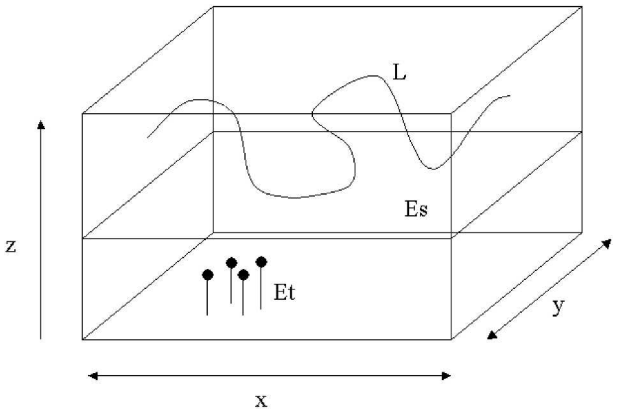

FIG. 1. Sketch of the different methods used in this study to calculate statistics. Eulerian statistics are calculated both in space (E_s) and in time (E_t), Lagrangian statistics (L) are calculated by following the particles' trajectories.

This definition gives the same result as (6) for an exponential autocorrelation, but it allows us to calculate more adequately the results for wavelike motion, like the vertical motion of a particle in the atmospheric CBL.

4. Eulerian statistics

Eulerian statistics are calculated in a fixed framework. Eulerian length and time scales have already been investigated in a large number of studies, both experimentally and numerically (e.g., Caughey and Palmer 1979; Hanna 1981; Lamb 1982; Deardorff and Willis 1985; Lenschow and Stankov 1986; Mason 1989). However, there is an essential difference between field experiments and numerical studies. Field experiments (e.g., Hanna 1981) usually provide temporal analysis (i.e., statistics derived by the analysis of time series collected at fixed positions), whereas in numerical (e.g., Mason 1989) or laboratory experiments (e.g., Deardorff and Willis 1985), data are collected at different locations at a fixed time (or averaged over a certain time); that is, spatial analysis is used. These two analyses are usually related by Taylor's hypothesis of frozen turbulence (Tennekes and Lumley 1972), which is always assumed but seldom validated. Here we analyze both time and spatial statistics in the Eulerian framework and evaluate the relationship between them.

a. Spatial analysis

One-dimensional spectra of the wind velocity components were obtained by Fourier transforming the LES results along the mean wind direction and then averaging them over all parallel lines. Each of these spectra was obtained from the model output every 10 min and then time averaged.

Figure 2 shows the normalized energy spectra for the wind velocity components calculated in the middle of the BL ($z/z_i = 0.50$). The LES results agree with the tank experiments by Deardorff and Willis (1985), the numerical results by Schmidt and Schumann (1989), and the wind tunnel data by Kaiser and Fedorovich (1998). As the figure shows, the numerical domain is sufficiently large to solve all the relevant scales of motion. In fact, the vertical profile of the velocity variances calculated as an integral of the spectra (not shown) are in agreement with previous experimental and numerical studies (Willis and Deardorff 1974; Lenschow et al. 1980; Dosio et al. 2003).

At short scales ($k/z_i > 20$), the slope of the spectra departs from the theoretical slope $k^{-5/3}$. This is a consequence of the finite numerical grid, as explained by Pasquill (1974). However, as mentioned earlier, the autocorrelation (and therefore the length scale) depends mainly on the larger scales, which are solved by the model. To investigate the dependence of the results on the smaller scale of motion, we performed a simulation

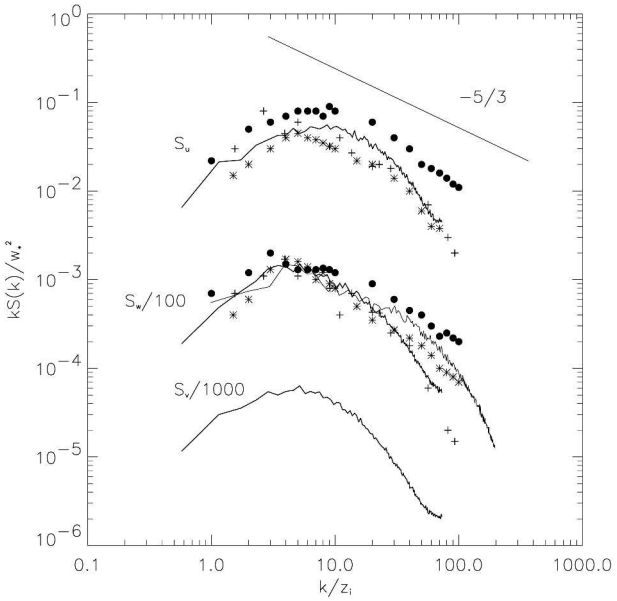

FIG. 2. Normalized energy spectra of the wind velocity components in the middle of the boundary layer ($z/z_i = 0.5$) calculated by spatial analysis (E_s). For clarity, the spectra have been divided by the factors shown near the curves. The following experimental data are also shown: * represents Deardorff and Willis (1985), + represents Schmidt and Schumann (1989), and ● represents Kaiser and Fedorovich (1998). The thin line represents the vertical velocity spectra for a simulation with a very fine uniform numerical grid ($10 \times 10 \times 10$ m).

using a very fine uniform numerical grid ($10 \times 10 \times 10$ m); the result (shown only for the vertical velocity) shows that, as expected, the shape (slope) of the spectrum at short scales is improved, but at large scales ($k/z_i < 20$), the shape of the spectrum and the magnitude and position of the spectral peak (which is proportional to the integral scale) are not modified. As was also pointed out by Schmidt and Schumann (1989), simulations with a different set of coefficients in the subgrid parameterization of their model showed a slight improvement in the spectra, but both the results at large scales and the agreement with measurements were not altered significantly.

Due to the scatter, it is not easy to estimate the wavelength Λ_j of the spectral peak. For the horizontal velocity, both Λ_u and Λ_v are generally in agreement with the relationship by Caughey (1982):

$$\Lambda_{u,v} = 0.15 z_i. \tag{12}$$

However, at heights $z/z_i > 0.8$, we found larger values for the wavelength, $\Lambda_{u,v} = 1.8 z_i$ at $z/z_i = 0.9$ and $\Lambda_{u,v} = 1.9 z_i$ at $z/z_i > 1$, respectively. For the vertical velocity, the vertical profile of Λ_w follows the curve,

$$\Lambda_w/z_i = 1.8[1 - \exp(-8z/z_i) - 0.0003 \exp(8.5z/z_i)], \tag{13}$$

which is similar to the expression suggested by Caughey and Palmer (1979) [as shown in Fig. 4a where the vertical profile of Λ_w/z_i is also compared with the atmospheric data by Caughey and Palmer (1979) and Graf and Schumann (1992), and the wind tunnel data by Kaiser and Fedorovich (1998)].

Figure 3 shows the autocorrelation function for the three wind components calculated at three different heights ($z/z_i = 0.1$, $z/z_i = 0.5$, and $z/z_i = 0.8$). The results are in agreement with the experimental data by Deardorff and Willis (1985) and the numerical experiment by Mason (1989). In the middle of the boundary layer, the autocorrelation function for w does not differ significantly from the autocorrelation functions for u and v. Near the surface layer and near the inversion, on the contrary, the autocorrelation function for the vertical velocity decays more rapidly than for the horizontal components.

This is corroborated by the vertical profiles of length scales λ_j (11), shown in Fig. 4b. Although a direct comparison is not possible due to the different definition of the length scale, our LES results agree with previous numerical studies (Mason 1989; Khanna and Brasseur 1998) and laboratory experiments (Deardorff and Willis 1985). The length scales remain approximately constant (with a variation of about 10% from the mean value) between $z/z_i = 0.2$ and $z/z_i = 0.7$. Lenschow and Stankov (1986) also showed that the profiles of the horizontal length scales remain constant with height.

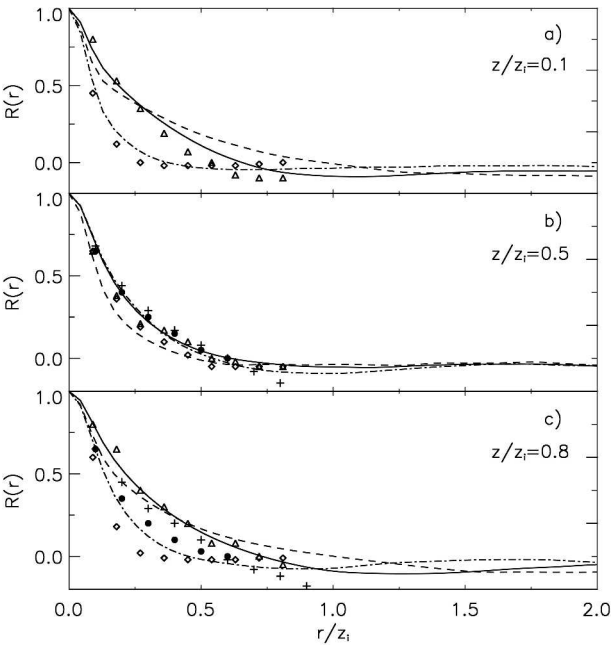

FIG. 3. Eulerian autocorrelation function $R^E(r)$ calculated according to (A4) at different heights as a function of the normalized space lag r/z_i. The continuous line is the u component, the dashed line is the v component, and the dashed–dotted line is the w component. The following experimental data are also shown: Δ and ◇ represent Mason (1989; u component and w component, respectively) and + and ● represent Deardorff and Willis (1985; u component and w component, respectively).

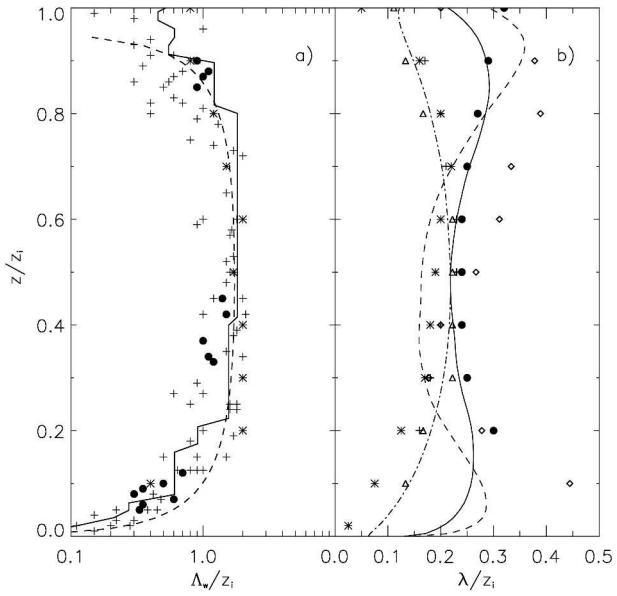

FIG. 4. (a) The continuous line is the vertical profile of the normalized length scale Λ_w (wavelength of the spectral peak) for the vertical velocity. The following experimental data are also shown: + represents Caughey and Palmer (1979), * represents Kaiser and Fedorovich (1998), and ● represents Graf and Schumann (1992). The dashed line is the parameterized curve (13). (b) Vertical profiles of the Eulerian length scale λ_j (normalized by the CBL height) calculated according to (11). The continuous line is the u component, the dashed line is the v component, and the dashed–dotted line is the w component. The following experimental data are also shown: * represents Khanna and Brasseur (1998), ● represents Mason (1989), and ◇ represents Deardorff and Willis (1985).

In the region below $z/z_i < 0.2$ and in the entrainment zone, the length scales differ significantly from their mean value in the bulk of the CBL. In particular, the vertical length scale decreases with height whereas the horizontal ones increase. As shown by previous studies (Mason 1989; Moeng and Rotunno 1990; Khanna and Brasseur 1998), the flow near the inversion zone is characterized by more isolated and discrete eddies, rather than large downdrafts surrounded by narrow updrafts, as in the middle of the CBL. Although the size of the eddies (updrafts) remains mostly constant with height, near the top of the CBL, there are fewer updrafts than at lower levels. This leads to a increase in the skewness of the vertical velocity in the inversion zone, as shown by Moeng and Rotunno (1990). They also showed that in a CBL characterized by a strong inversion, the updrafts convert part of their kinetic energy into that of the horizontal velocity field; as a result, vertical motion is converted into horizontal motion.

The results of Lenschow and Stankov (1986) show that the horizontal length scale maintains a more constant profile near the top of the CBL, and the vertical length scale continues growing with height. Their results were obtained as an average of measurements for different boundary layers, with values of the shear/buoyancy ratio u_*/w_* varying from 0.18 to 0.46 and the stability parameter $-z_i/L$ varying from 7.5 to 54. It is therefore possible that wind shear influenced the results in some cases. As shown by Carruthers and Hunt (1986), the values of the length scales depend on the atmospheric stability of the upper layer. Mason (1989) also observed that the results by Lenschow and Stankov (1986) near the top of the CBL could have been influenced by the presence of large-scale motion in the stable layer above the inversion.

b. Temporal analysis

Time series for the three velocity components were collected at 1024 points uniformly distributed in the horizontal domain for each vertical level. Spectra were subsequently calculated and averaged over the points (horizontal space average over the whole domain).

Figure 5 shows the energy spectra for the wind velocity components calculated in the middle of the CBL ($z/z_i = 0.5$). In spite of the large scatter in the observations, our results agree qualitatively with the atmospheric data by Caughey and Palmer (1979; although they show spectra only at $z/z_i = 0.9$). As explained earlier, also in this case the fall of the spectra from the theoretical slope at small scales (large frequencies) is a consequence of the time step used, but it does not influence the values of the autocorrelations and time scales.

The autocorrelations for the three wind components at different heights are shown in Fig. 6 and the vertical

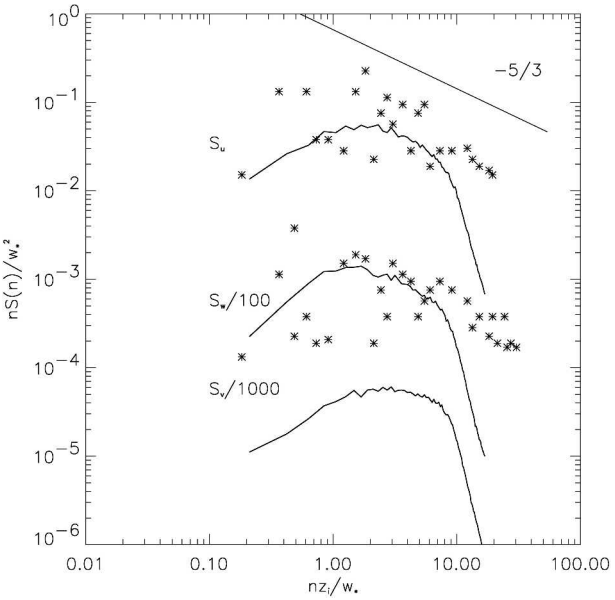

FIG. 5. Normalized energy spectra of the wind velocity components in the middle of the boundary layer ($z/z_i = 0.5$) calculated by temporal analysis (E_t). For clarity, the spectra have been divided by the factors shown near the curves. The atmospheric data by Caughey and Palmer (1979) are also shown (*).

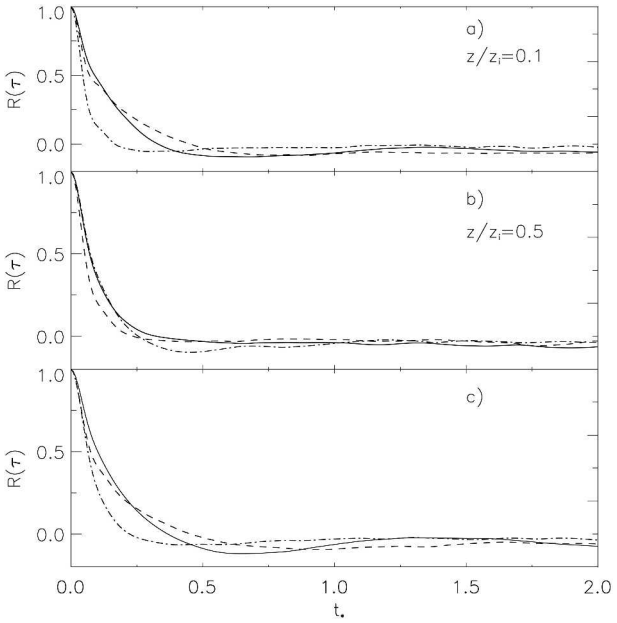

FIG. 6. Eulerian autocorrelation function $R^{\mathrm{E}}(\tau)$ calculated according to (A1) at different heights as a function of the nondimensional time lag t_*. The continuous line is the u component, the dashed line is the v component, and the dashed–dotted line is the w component.

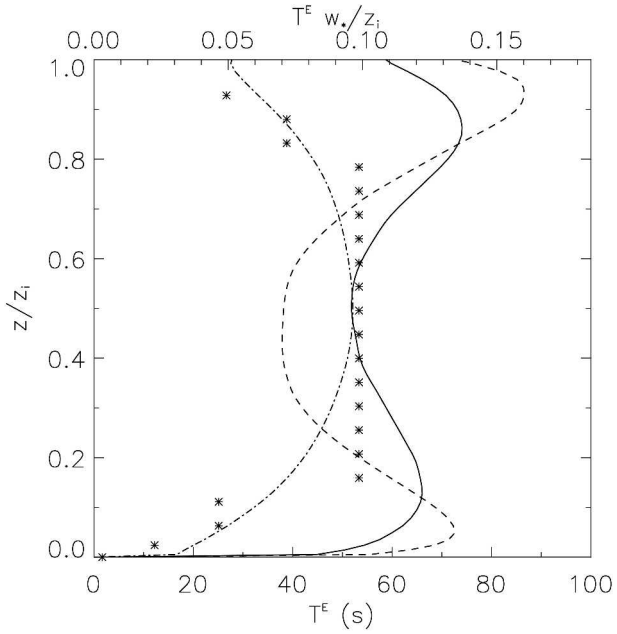

FIG. 7. Vertical profiles of the Eulerian time scale T_j^{E} calculated according to (11). The continuous line is the u component, the dashed line is the v component, and the dashed–dotted line is the w component. In the figure, the Eulerian time scale for the vertical wind component calculated according to (14) is also shown (*).

profiles of time scales T_j^{E} calculated according to (11) are shown in Fig. 7. Both the autocorrelation and the integral-scale profiles have similar values and vertical shape to the ones calculated through spatial analysis (Figs. 3 and 4). Atmospheric measurement of Eulerian integral time scales for convective conditions ($-z_i/L$ ranging from -20 to -375) are reported by Hanna (1981), although no vertical profiles are shown. In his work, averaged values of $T_u^{\mathrm{E}} \sim 44$ s and $T_w^{\mathrm{E}} \sim 55$ s are reported, and they agree with the LES results.

Here, it is worth mentioning that the integral scales can be also calculated directly from the spectra. In fact, assuming an autocorrelation with an exponential shape Hanna (1981) showed that

$$T^{\mathrm{E}} \sim \frac{1}{6} T_m, \tag{14}$$

where T_m is the period at which spectral peak occurs. Although a precise determination of the spectral peak is difficult, relationship (14) is generally well satisfied for all the wind components. For instance, values of the integral scales calculated at $z/z_i = 0.5$ according to (14) are $T_u^{\mathrm{E}} = 56$ s, $T_v^{\mathrm{E}} = 34$ s, and $T_w^{\mathrm{E}} = 53$ s. In Fig. 7, the vertical profile of T_w^{E} calculated according to (14) is plotted, showing that the agreement is very satisfactory. However, as pointed out by Hanna (1981), the determination of the integral scale from the autocorrelation function is preferable, as it leads to more accurate results.

c. *Validation of Taylor's hypothesis of frozen turbulence in atmospheric flows*

As mentioned earlier, field experiments usually measure variables that evolve with time. In laboratory experiments and numerical simulations, on the other hand, spatial analysis is often used. The two frameworks are related by Taylor's hypothesis of frozen turbulence. Following Pasquill (1974), Taylor's hypothesis is applied to autocorrelations and spectra as follows:

$$R(t) = R(x) \quad \text{if } x = Ut, \tag{15}$$

$$US(n) = S(k) \quad \text{if } n = Uk. \tag{16}$$

This in turn leads to the relationship between Eulerian length and time scales,

$$UT^{\mathrm{E}} = \lambda^{\mathrm{E}}, \tag{17}$$

where U is the (height dependent) mean wind in the x direction (along which data are collected). As explained earlier, in the simulated strongly convective CBL, the wind profile is mostly constant between $z/z_i = 0.1$ and $z/z_i = 0.9$. The length scales λ^{E} and time scales T^E are calculated from both autocorrelation functions and spectra through (11) and (14), respectively. To our knowledge, this is the first time that length and time scales are calculated with two independent methods within the same experiment, allowing a direct validation of relation (17). The vertical profile of the ratio $1/U\ \lambda^{\mathrm{E}}/T^{\mathrm{E}}$, calculated by combining the results

shown in Figs. 4 and 7, is close to 1 for all the wind components, which shows that Taylor's hypothesis [relationships (15) and (16)] holds in the simulated CBL. Only in the regions very close to the surface ($z/z_i < 0.05$) and at the top of the CBL ($z/z_i > 0.95$), where a strong wind shear is present, is the ratio $1/U\ \lambda^E/T^E$ slightly different than 1, being 1.2 and 0.8, respectively.

5. Lagrangian statistics

Lagrangian statistics were calculated by following, both in space and in time, the particles released at different positions in the simulated CBL. In Fig. 8, an example of a particle trajectory [i.e., vertical position as a function of the nondimensional time $t_* = (z_i/w_*)t$] is shown. The particle is released in the middle of the boundary layer ($z/z_i = 0.5$) and is rapidly caught by the thermals that transport it in a wavelike motion between the boundaries of the CBL. This motion is typical of meandering plumes in a strongly convective boundary layer.

In the same picture, the mean plume height (plume centerline) of particles released at three different heights ($z/z_i = 0.2$, 0.5, and 0.85, respectively) is also shown. The vertical motion at short times after the release ($t_* < 1$) is largely dependent on the release height. As shown, particles released at $z/z_i = 0.2$ are caught by the updrafts and rise very quickly, whereas particles released at $z/z_i = 0.8$ descend more slowly and remain in the upper part of the CBL for a long time. The difference in the particles' motions at short times is related to the different vertical structure of the turbulent flow at different heights of the CBL and to the conversion of vertical motion into horizontal motion due to the strong inversion at the top of the CBL, as explained earlier.

At longer times ($t_* > 2$), all particles are (on average) in the middle of the CBL, and therefore they have a similar behavior, moving in a periodic motion between the boundaries of the CBL.

In short, the vertical inhomogeneity of the flow influences the particle motion at short times, whereas the presence of the CBL boundaries affects the particles' motion at longer time. As will be discussed later, these two effects have a direct influence on the shape of the autocorrelation and consequently on the values of the Lagrangian time scale.

Figure 9 shows the spectra of the vertical velocity for a particle released in the middle of the CBL. As explained by Corssin (1963), the Lagrangian spectra in the inertial subrange follows a n^{-2} slope. With respect to the Eulerian one, the peak shifts toward smaller frequencies, as shown by Hanna (1981). The value of the spectral peak frequency with respect to the one calculated in the Eulerian framework will be discussed later. Lagrangian autocorrelations calculated using (A5) are shown in Fig. 10 as a function of the dimensionless time t_*. To have statistically sound results, they are presented as an average over particles released at three different heights: particles released below $z/z_i = 0.25$ (10 240 particles), particles released between $z/z_i = 0.25$ and $z/z_i = 0.75$ (30 720 particles), and particles released above 0.75 (10 240 particles).

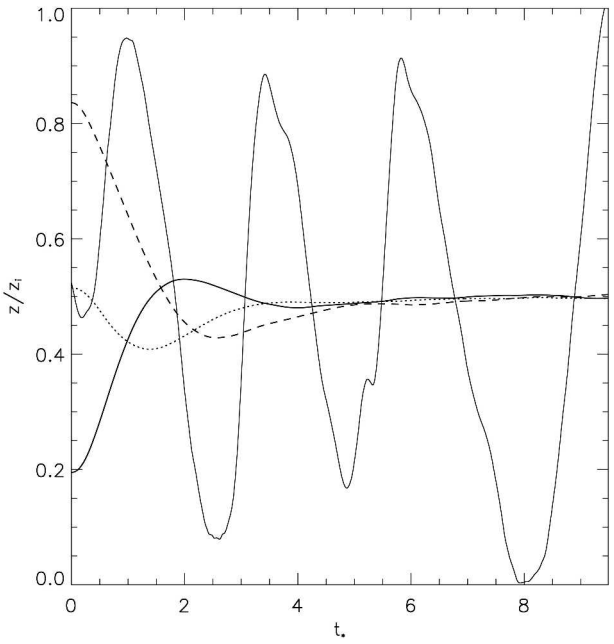

FIG. 8. Mean plume height (plume centerline) of particles released at three different heights ($z/z_i = 0.2$, 0.5, 0.85, respectively) and example of an individual trajectory (vertical position as function of time) of a particle released at $z/z_i = 0.5$.

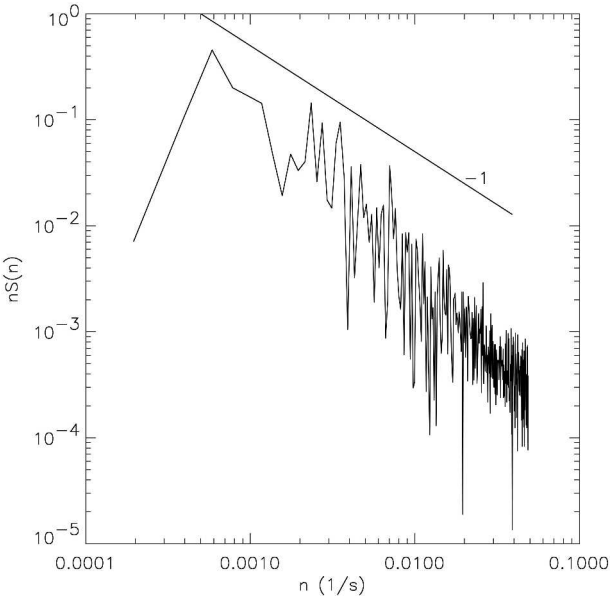

FIG. 9. Lagrangian energy spectra of the vertical velocity for a particle released in the middle of the boundary layer.

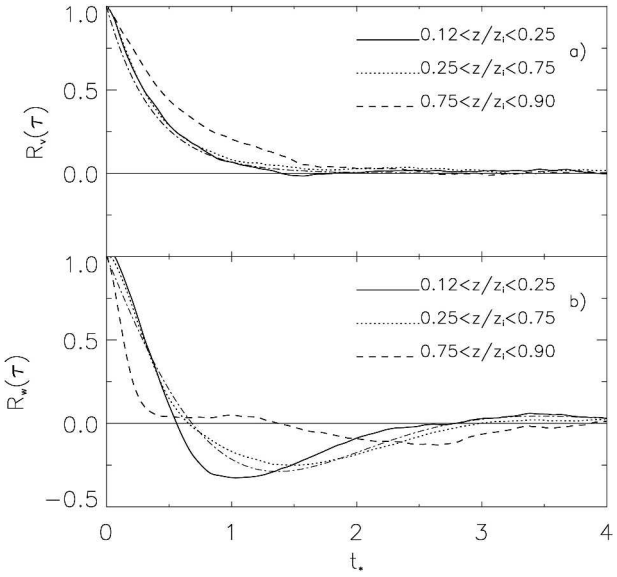

FIG. 10. (a) Lagrangian autocorrelation for the horizontal (v) motion for particles released at different heights. The function $R(\tau) = \exp(-\tau/200)$ is also shown (dashed–dotted line). (b) Lagrangian autocorrelation for the vertical (w) motion for particles released at different heights; (18) is also shown (dashed–dotted line).

There is a noticeable difference between the autocorrelation for the horizontal (v) and the vertical (w) wind component. The horizontal autocorrelation (Fig. 10a) closely follows an exponential decay [i.e., at $z/z_i = 0.5$ $R(\tau) = \exp(-\tau/200)$], characteristic of a Markov process. The shape of the autocorrelation is independent of the height of the release, but it is clear that the integral of the autocorrelation for particles released above $z/z_i = 0.75$ is slightly larger than the one for particles released in the middle of the CBL.

The vertical autocorrelation departs from an exponential function. The shapes of the autocorrelation of particles released below $z/z_i = 0.25$ or between $z/z_i = 0.25$ and $z/z_i = 0.75$ are quite similar and peculiar. Both have a strong minimum (at $t_* = 1$ and 1.4, respectively), and they reach constant value close to zero at larger times. This particular shape of the autocorrelation is found for periodic (or wavelike) motions, as explained by Csanady (1973). In the CBL, the particles' vertical motion is limited by the bottom and the top boundaries, and the particles move periodically within the CBL, as shown in Fig. 8. This autocorrelation is reproduced analytically by combining a stochastic motion (characterized by an exponential autocorrelation) and a wavelike motion (characterized by a sinusoidal autocorrelation). The resulting autocorrelation has a shape similar to the analytical function (Csanady 1973),

$$R^{\mathrm{L}}(\tau) = e^{-m\tau}\left[\cos(n\tau) - \frac{m}{n}\cos(n\tau)\right]. \qquad (18)$$

As Fig. 10b shows, the function (18) with $m = 0.9$ and $n = 1.5$ fits the LES results accurately for the release at $z/z_i = 0.5$.

As mentioned previously, experimental measurements of Lagrangian statistics in the CBL are extremely rare. In his study, Hanna (1981) calculated the integral time arbitrarily assuming that T_L corresponds to the time lag at which $R(\tau)$ first drops to 0.37, therefore implicitly assuming an exponential shape for $R(\tau)$. However, he pointed out that the autocorrelation curves do not approach zero at the largest time lags available. This may implicate that his dataset (30 min record) was too short to show the negative behavior of the autocorrelation function at large times.

In their study of synoptic-scale Lagrangian autocorrelation function, Daoud et al. (2003) analyzed a large database of modeled 10-day atmospheric trajectories, and they showed indeed an autocorrelation function whose shape is similar to that in our study (although in their case, it is the horizontal velocity autocorrelation). They also related this shape to wavelike motion of the particle in the atmosphere.

Numerical investigations of Lagrangian statistics in turbulent flow are reported by Wang et al. (1995) and Yeung and Pope (1989). The latter performed a direct numerical simulation of isotropic turbulence at a relatively low Reynolds number (<100); therefore their study is not directly comparable with atmospheric turbulence. Wang et al. (1995) performed an LES simulation of a turbulent channel flow at a Reynolds number of 21 900, which can be regarded as an idealization of a neutral atmospheric boundary layer. In our opinion, particles released in a neutral BL have a different behavior compared to a pure convective CBL. As shown by Dosio et al. (2003), a tracer released in a near-neutral BL is transported horizontally rather than vertically; the vertical dispersion is reduced whereas the horizontal dispersion is enhanced. Therefore, the vertical wavelike motion, which leads to the negative-shaped autocorrelation, is largely reduced in a neutral BL. In fact, as Fig. 10b shows, the shape of the autocorrelation for particles released above $z/z_i = 0.75$ (where the turbulence characteristics are different than in the bulk of the CBL) is much closer to an exponential shape, especially at short time. At longer time ($t_* > 2$), when the particles are in the middle of the CBL, the autocorrelation shows the negative minimum (but smaller than the other cases), and finally it reaches zero.

From the autocorrelation function, the following function is calculated:

$$T_j^{\mathrm{L}}(t) = \int_0^t R_j^{\mathrm{L}}(\tau)d\tau. \qquad (19)$$

By definition (6), the Lagrangian time T_j^{L} is therefore the limit for large times of $T_j^{\mathrm{L}}(t)$.

Figure 11 shows the function $T_j^L(t)$ for the horizontal and vertical motion as a function of t_*. For the horizontal motion, $T_v^L(t)$ grows constantly until it reaches a (fairly) constant asymptotic value. This asymptote represents the Lagrangian time (6), and it has a value $T_v^L = 230$ s for particles released between $z/z_i = 0.25$ and $z/z_i = 0.75$. The time at which the autocorrelation drops to $1/e$ is $T_e = 200$ s. Such small discrepancy is due to statistical errors related to the small fluctuations around zero for large time lags ($2 < t_* < 4$) (Fig. 10a). In fact, as shown in Fig. 10a, the analytical function $R(\tau) = \exp(-\tau/200)$ fits very well the autocorrelation calculated by the LES. The Lagrangian time for particles released above $z/z_i = 0.75$ has a larger value ($T_v^L = 310$ s, as explained previously.

For the vertical motion, the curve $T_w^L(t)$ follows closely the one for the horizontal motion for short times ($t_* < 0.5$) before reaching a maximum and finally dropping to zero. The value and the position of the maximum depend on the release height, being $T_w^L = 175$ s for particles released above $z/z_i = 0.75$ and $T_w^L = 100$ s for particles released above $z/z_i = 0.75$.

It is therefore clear that in the atmospheric CBL, the Lagrangian properties at short times depend on the release height, due to the turbulence vertical structure. Moreover, a peculiar difference exists at large times between vertical and horizontal direction, due to the limitation by the lower and upper boundaries to the vertical motion. These effects have a large influence on the autocorrelation shape and the value of the Lagrangian time, as shown. This difference between horizontal and vertical motion has also a great effect on the particle displacement (dispersion), as will be discussed in the next section.

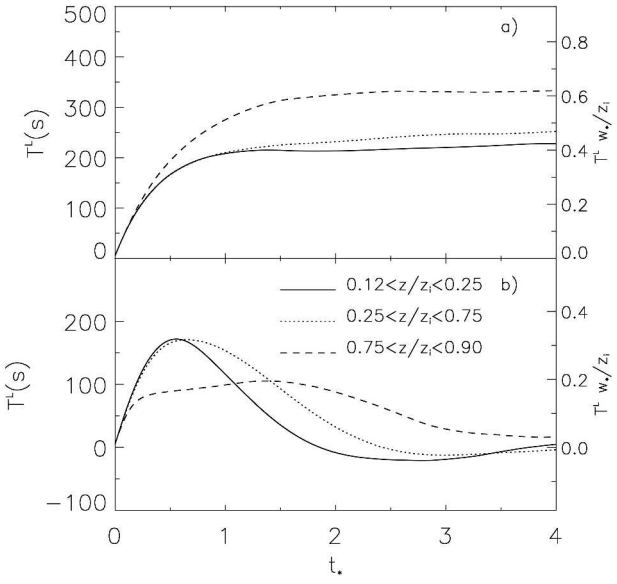

FIG. 11. Integral of the autocorrelation (19) for the (a) horizontal and (b) vertical wind components for particles released at two different heights (continuous line: $z/z_i = 0.5$; dashed line: $z/z_i = 0.85$).

6. Horizontal and vertical dispersion

In this section, the relationship between the flow properties and the dispersion characteristics is analyzed. In particular, dispersion characteristics are calculated in both Eulerian and Lagrangian frameworks. Taylor's relation [(2)] relates the autocorrelation $R(\tau)$ to the particles' displacement $\overline{x_j'^2}(t)$ (1); both of these quantities are calculated in the Lagrangian framework. As pointed out by Blackadar (1998), for practical applications the Lagrangian quantity (1) is often replaced with the Eulerian one $\sigma_{x_j}^2$. The latter refers to the standard deviation of the position of all the particles that lie at distance $X = Ut$ downwind of the source, whereas $\overline{x_j'^2}(t)$ refers to all the particles that have traveled a time t since leaving the source. Some of them will be situated closer and some farther from the source than the distance X. In practical application, the Eulerian quantity $\sigma_{x_j}^2$ is calculated (measured) instead of the Lagrangian $\overline{x_j'^2}(t)$, assuming that the difference is not very great.

By using the LES results, we calculate both $\sigma_{x_j}^2$ and $\overline{x_j'^2}(t)$ and compare them with Taylor's relationship (2). To calculate the Eulerian dispersion, particles are tracked as a function of space, instead of time, and $\sigma_{x_j}^2$ is calculated at intervals equal to the grid size from the initial position. The results are shown in Figs. 12 and 13 and are discussed below.

a. Horizontal dispersion

For the horizontal motion (Fig. 12), Taylor's theory is satisfactorily fulfilled. The Lagrangian displacement $\overline{y'^2}(t)$ is similar to the Eulerian dispersion parameter σ_y^2, and both agree with previous studies and laboratory measurements (Lamb 1978; Willis and Deardorff 1981). Equation (2) closely follows the displacement curves, and it shows the expected limits at short and long times, respectively, $\sigma_v t$ and $2\sigma_v(T_v^L t)^{1/2}$. This satisfactory agreement is closely related to the exponential shape of the autocorrelation (Fig. 10), leading to a constant limit at longer times for the value of the Lagrangian integral time (Fig. 11).

b. Vertical dispersion

The results for the vertical dispersion are shown in Fig. 13. It is first important to notice that also in this case, the Lagrangian displacement $\overline{z'^2}(t)$ and the Eulerian dispersion parameter σ_z^2 are very similar, which implies that, for practical purposes, using Eulerian dispersion parameters instead of the Lagrangian one does not lead to large errors. This is related to the fact that Taylor's hypothesis of frozen turbulence holds in the simulated CBL, as shown before. As a result, dispersion statistics calculated for particles that traveled a time t

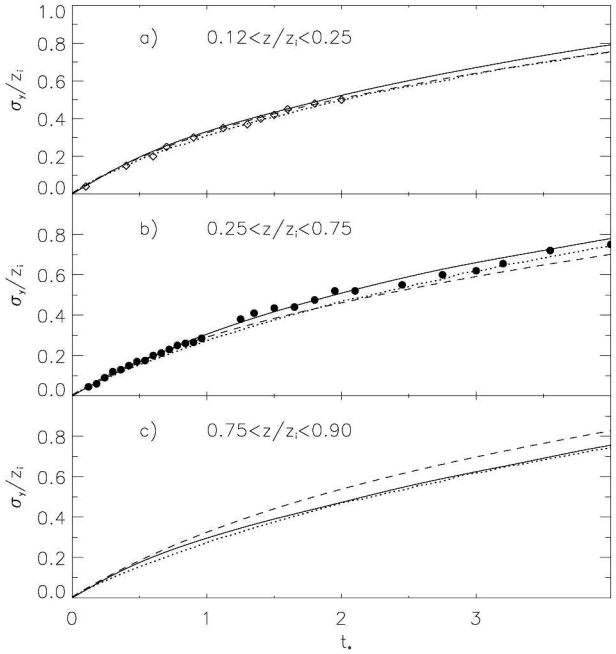

FIG. 12. Normalized horizontal dispersion parameters as a function of the dimensionless time t_*. The continuous lines are the Lagrangian displacements $\overline{y'^2}(t)$ (1), the dotted lines are the Eulerian dispersion parameters σ_y, and the dashed lines represent Taylor's theory (2). (a) Horizontal dispersion for particles released below $z/z_i = 0.25$. Data (◇) from the numerical experiment by Lamb (1978) are also shown. (b) Same as in (a), but for particles released between $z/z_i = 0.25$ and $z/z_i = 0.75$. The water tank data (●) from Willis and Deardorff (1981) are also shown. (c) Same as in (a), but for particles released above $z/z_i = 0.75$.

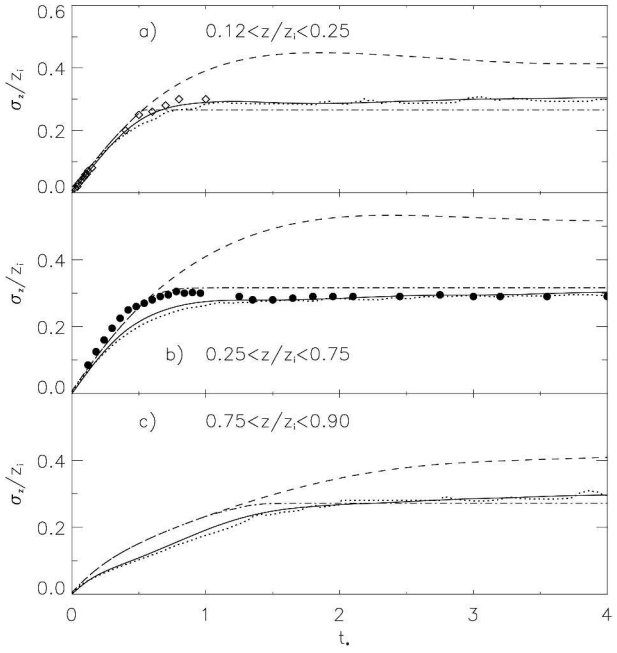

FIG. 13. Normalized vertical dispersion parameters as a function of the dimensionless time t_*.The continuous lines are the Lagrangian displacements $\overline{z'^2}(t)$ (1), the dotted lines are the Eulerian dispersion parameters σ_z, and the dashed lines represent Taylor's theory (2). (a) Vertical dispersion parameters for particles released below $z/z_i = 0.25$. The dashed–dotted line represents expression (2) calculated using the function $T'_L(t)$. Data (◇) from the numerical experiment by Lamb (1978) are also shown. (b) Same as in (a), but for particles released between $z/z_i = 0.25$ and $z/z_i = 0.75$. The water tank data (●) from Willis and Deardorff (1981) are also shown. (c) Same as in (b), but for particles released above $z/z_i = 0.75$.

after the release are equivalent to those calculated for particles that lie at distance $X = U/t$ from the source.

However, for the vertical motion, the comparison between the particle displacement and Taylor relationship (2) is less satisfactory and requires a more detailed analysis and discussion. Since the shape of the vertical autocorrelation function and the Lagrangian time depend on the particle release height, the results are presented separately for particles released below and above $z/z_i = 0.75$.

1) PARTICLES RELEASED BELOW $Z/Z = 0.75$

The vertical displacement (1) calculated from the particle trajectories agrees with previous experiments (Lamb 1978) and reaches a constant limit of $\overline{z'^2}(t) \sim 0.3$, characteristic of an ensemble of particles uniformly mixed within the CBL. Equation (2), on the other hand, agrees with the displacement and previous experiments only at short times ($t_* < 0.7$). This time is of the same order of magnitude as the turnover time and corresponds to the period when the particles, just after being released, are still unaffected by the CBL boundaries. In other words, the particles are in a regime of "free motion."

As Fig. 13b shows, at longer times, (2) reaches a constant limit of about 0.5. This limit is due to the peculiar shape of the autocorrelation for vertical motion for $t_* > 2$, which leads to $T_w^{\mathrm{L}} = \lim_{t\to\infty} T_w^{\mathrm{L}}(t) \simeq 0$ (see Fig. 11b). As a result, (2) becomes

$$\overline{x_j'^2}(t) \sim \int_0^t \int_0^{t'} R_w^{\mathrm{L}}(\tau)\, d\tau\, dt' = \int_0^t T_w^{\mathrm{L}}(t')\, dt' = \text{constant}. \tag{20}$$

As mentioned earlier, Taylor's diffusion theory was developed for homogeneous turbulence, whereas the CBL is characterized by vertically inhomogeneous turbulence. Moreover, the vertical motion is bounded by the CBL boundaries, and in strongly convective conditions, the particles are transported in a wavelike motion as shown in Fig. 8. Therefore, we consider it more appropriate to make a distinction between free and bounded motion, as discussed later.

2) PARTICLES RELEASED ABOVE $z/z_i = 0.75$

The displacement of particles released above $z/z_i = 0.75$ is strongly affected by the turbulent structure in the

upper part of the CBL. As discussed previously, the turbulence structure near the top of the CBL is different than in the lower layers, due to the strong capping inversion, and vertical motion is converted into horizontal motion. As a result, at short times, when the particles have not yet reached the middle of the CBL, the vertical displacement is diminished. At longer times ($t_* > 3$), the particles are well mixed within the entire CBL, and the displacement (1) reaches the constant limit of about 0.3 as explained earlier. However, also in this case, (2) overestimates this limit at longer times (Fig. 13c).

3) Distinction between free and bounded motion

A more adequate interpretation of the LES results with respect to (2) is obtained if the two regimes (free motion and bounded motion) are considered separately, or in other words, when a distinction is made between shorter and longer times after the release.

As previously shown, the period of time in which the particles are in a regime of free motion (before being affected by the CBL boundaries) is of the same order of magnitude as the turnover time. If t_0 is the time at which the function $T_w^{\mathrm{L}}(t)$ reaches its maximum value, then $T_w^{\mathrm{L}}(t_0) = T_w^{\mathrm{L}}$ according to (11). A new time scale is defined as

$$\begin{cases} T'_L(t) = T_w^{\mathrm{L}}(t) & t \le t_0 \\ T'_L(t) = 0 & t > t_0 \end{cases}. \tag{21}$$

The function $T'_L(t)$ is shown in Fig. 14 for particles released at $z/z_i = 0.5$ and $z/z_i = 0.85$. This function is consistent with the two limits (for shorter and longer times) that the function $T_w^{\mathrm{L}}(t)$ must fulfill.

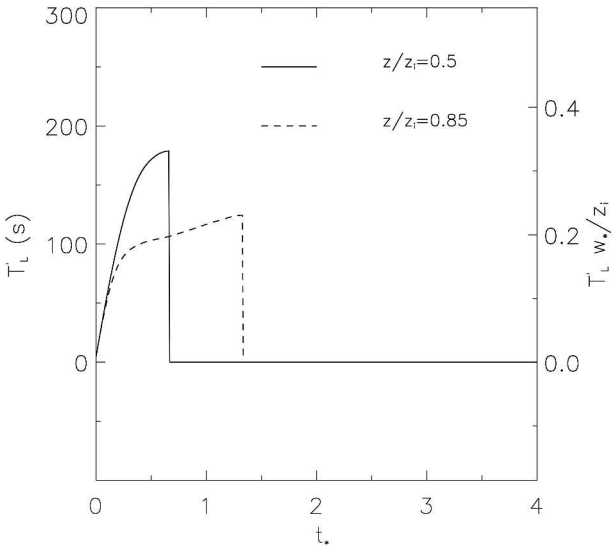

FIG. 14. Time scale $T'_L(t)$ (21) for particles released at $z/z_i = 0.5$ (continuous line) and $za/z_i = 0.85$ (dashed line).

If we now recalculate (2) using the new function $T'_L(t)$, the result agrees more satisfactorily with the experiments and the particle displacement $\overline{z'^2}$, as shown in Fig. 13.

7. Relationship between Eulerian and Lagrangian frameworks

In this section, we derive relationships between the Lagrangian and Eulerian frameworks from the LES results for the autocorrelation functions and spectra.

a. Integral Lagrangian time scale

Figures 15a and 15c show the vertical profiles of time scales T_j^{L} calculated from the autocorrelation functions according to (11). Both the horizontal and vertical Lagrangian time scales are almost constant with height for $z/z_i < 0.7$. The vertically averaged values below $z/z_i < 0.7$ are $T_v^{\mathrm{L}} = 220$ s and $T_w^{\mathrm{L}} = 180$ s, respectively. As explained earlier, the Lagrangian time scale can also be calculated directly from the spectra, using an expression similar to (14). By using this method, averaged values of $T_v^{\mathrm{L}} = 235$ s and $T_w^{\mathrm{L}} = 210$ s are found, which shows that the two ways of determining T_j^{L} are equivalent. However, the determination of the integral time by the spectral technique leads to greater uncertainties due to the difficulty in precisely locating the spectral peak.

Our results are in agreement with the measurements by Phillips and Panofsky (1982) ($T_v^{\mathrm{L}} \sim 190$ s). Other previous experimental studies show a large uncertainty in the value of the Lagrangian time. For instance, atmospheric measurements range from 70–80 s (Hanna 1981) to 10^4 s (Gifford 1982). The numerical studies by Wang et al. (1995) and Uliasz and Sorbjan (1999) do not provide a direct value of the calculated integral time scale. As pointed out by Hanna (1981), atmospheric measurements are influenced by the complexity of the experimental setup and the short sampling time. Moreover, the results depend on different meteorological conditions during the measurement campaign. The LES results, on the contrary, are obtained from a more controlled experiment and a longer time series of data.

The value of the Lagrangian time scale is commonly parameterized as a function of CBL Eulerian characteristics (Angell 1964). In particular, T_j^{L} is related to the wavelength of the spectral peak Λ_j according to (Degrazia et al. 1998)

$$T_j^{\mathrm{L}} = \frac{\sqrt{\pi}}{16}\frac{\Lambda_j}{\sigma_j}. \tag{22}$$

By substituting in (22) the values of Λ_j calculated by the LES [(12) and (13)], the following relationships are found:

$$T_v^{\mathrm{L}} = 0.17\,\frac{z_i}{\sigma_v} \quad \text{and} \tag{23}$$

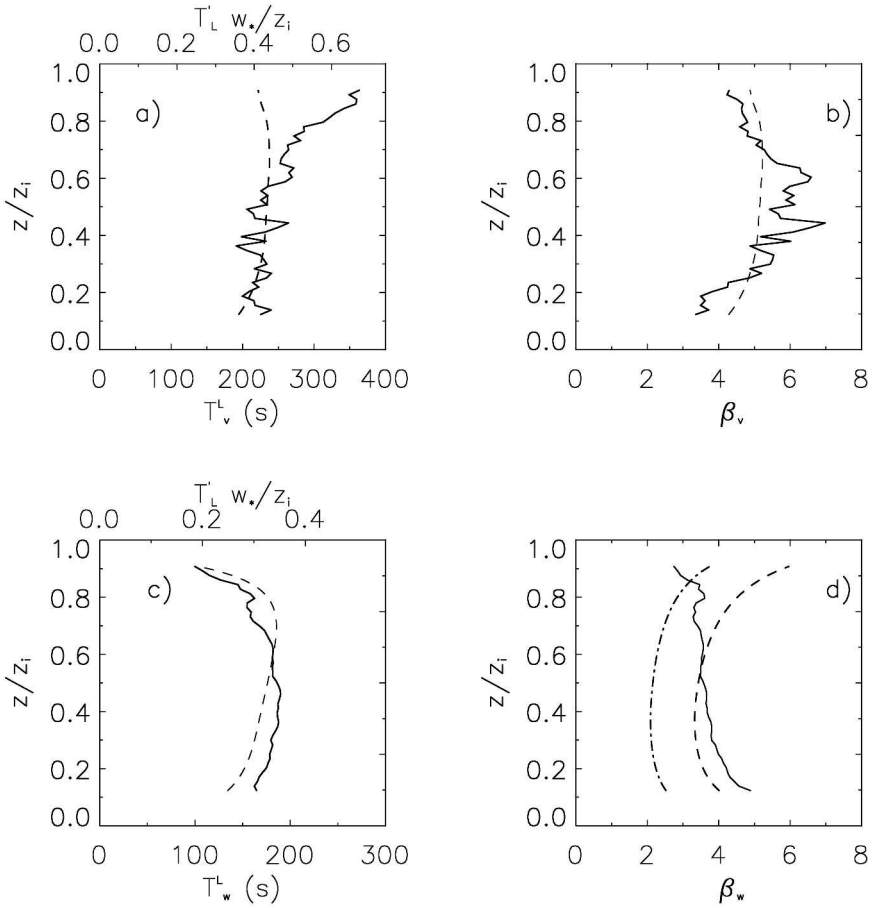

FIG. 15. (a) Vertical profiles of horizontal Lagrangian time scale as calculated by LES (continuous line) and parameterized according to (23) (dashed line). (b) Ratio between the horizontal Lagrangian and Eulerian time scales as calculated by LES (continuous line) and parameterized according to (25) (dashed line). (c) Same as in (a), but for the vertical wind component. (d) Same as in (b), but for the vertical wind component.

$$T_w^{\mathrm{L}} = 0.2\,\frac{z_i}{\sigma_w}\,[1 - \exp(-8z/z_i) - 0.0003\exp(8.5z/z_i)]. \tag{24}$$

As shown by Degrazia et al. (1998), (23) and (24) agree with the atmospheric measurements by Hanna (1981) in the middle of the CBL. In Figs. 15a and 15c, (23) and (24) are compared with the LES results. Both parameterizations are able to reproduce the LES results correctly for heights below $z/z_i = 0.7$.

Above $z/z_i = 0.7$, the LES results show an increase of T_v^{L} with height (Fig. 15a). This is consistent with the calculation of the integral time scale from the spectral peak, which shows an averaged (above $z/z_i = 0.7$) value of $T_v^{\mathrm{L}} = 260$ s. As discussed in section 4a, the value of the wavelength Λ_j calculated by the LES is $\Lambda_{u,v} = 1.8z_i$ at $z/z_i = 0.9$ and $\Lambda_{u,v} = 1.9z_i$ at $z/z_i = 1$. If these values are used in (22), a better agreement is found between the LES results and the parameterization.

b. *Value of the ratio* β_j

Figures 15b and 15d show the ratio β_j of the Lagrangian to Eulerian time scales for the horizontal and vertical wind components. For the horizontal wind component, β_v varies between 4 and 6, with a vertically averaged value of $\beta_v = 5$. The irregular vertical profile of β_v is due to fluctuations in the autocorrelation function (Fig. 10a). For the vertical wind component, the values of β_w calculated by the LES have a vertically averaged value of 4. Values in literature range form 1.8 (Hanna 1981) to 4 (Angell 1964).

The value of β_j is usually related to the intensity of turbulence $i = \sigma_j/U$ by (9), as explained previously. In Fig. 15b, the following parameterization proposed by Hanna (1981) is also shown:

$$\beta_j = C\,\frac{U}{\sigma_j} = 0.7\,\frac{U}{\sigma_j}. \tag{25}$$

As it can be seen, despite the fluctuations, the pa-

rameterization is in satisfactory agreement with the LES results.

As shown in Fig. 15d, the parameterization (25) for the vertical component agrees with the LES results only for $z/z_i < 0.7$. Other values of the constant C range in the literature from 0.35 to 0.8 as reported by Pasquill (1974). Theoretical analysis by Wandel and Kofoed-Hansen (1962) leads to $C = 0.44$ whereas the numerical simulation by Wang et al. (1995) gives a value of $C = 0.6$. To illustrate the dependence of the parameterization on the value of the constant C, (25) is shown in Fig. 15d for two values of the constant, $C = 0.4$ and $C = 0.7$, respectively. As stated by Hanna (1981), the value $C = 0.7$ gives the best fit for the overall dataset, whereas the value $C = 0.4$ fits the experimental data for high wind speed better, and it is in better agreement with the LES results for $z/z_i > 0.7$.

8. Conclusions

Eulerian and Lagrangian statistics were calculated by means of an LES. A large numerical domain and a long integration time were used in order to obtain reliable statistics both in space and in time. The flow characteristics were studied by analyzing the energy spectra and velocity autocorrelations in both the Eulerian and Lagrangian frameworks.

Three main research issues were studied. First, Eulerian statistics were calculated by means of spatial and temporal analyses. The two frameworks are related by Taylor's hypothesis of frozen turbulence. Characteristic length and temporal scales were derived by means of two different methods, namely through the analysis of the autocorrelation function and the spectral peak, allowing a direct validation of Taylor's hypothesis, the results of which were satisfied in the simulated CBL.

Second, the relationship between flow properties (autocorrelations) and dispersion characteristics (particles' displacements) was discussed through Taylor's analysis of turbulent dispersion. Results showed that for the horizontal velocity, the autocorrelation had an exponential shape, characteristic of a stochastic motion. As a result, horizontal dispersion was satisfactorily described by Taylor's diffusion theory. On the contrary, the autocorrelation function for the vertical velocity had a more complicated shape, due to the vertical inhomogeneity of the turbulent flow. Moreover, the particle vertical motion is confined between the CBL boundaries. As a result, particles moved following a wavelike motion, and the value of the integral scale was zero. Taylor's analysis correctly predicted the particles' displacement at short times but overestimated the asymptotic limit at longer times.

The use of a different method to calculate the Lagrangian integral time (11), allowed us to distinguish better between free and bounded motion, and a better agreement between Taylor's relationship and particles' vertical displacement was found.

This study was completed by verifying the equivalence between Lagrangian particle displacement $\overline{x_j'^2}$ and the Eulerian dispersion parameter $\sigma_{x_j}^2$. The comparison showed that, for practical purposes, using Eulerian dispersion parameters instead of the Lagrangian one does not lead to large errors. This is related to the fact that Taylor's hypothesis of frozen turbulence holds in the simulated CBL.

Finally, the relationship between Lagrangian and Eulerian framework was investigated through the calculation of the Lagrangian integral scales and the ratio β. Vertical profile of T_j^L showed that the integral scales remain constant at heights $z/z_i < 0.7$. The difference in the turbulence characteristics near the inversion influenced the particles' motion, which is transformed from vertical into horizontal. This affected the values of the integral scales in the upper layers of the CBL, where the horizontal time scale increased, whereas the vertical time scale was reduced. Currently used parameterizations for the ratio β, derived either in previous field atmospheric experiments or through theoretical analysis, were compared with the LES results, showing a satisfactory agreement. The present study indicates the need for further investigation on the values of time and length scales near the inversion zone ($z/z_i > 0.7$) of the CBL and their implication for atmospheric dispersion.

Acknowledgments. Discussions and comments by Stefano Galmarini, Harm Jonker, Han van Dop, Arjan van Dijk, and Jeffrey C. Weil have been very useful and are deeply appreciated. A. Dosio is funded within the Centre of Expertise Emissions and Assessment—a cooperation between TNO and Wageningen University. All the numerical simulations have been performed on the TERAS supercomputer of the National Computing Center SARA (Project Number 2003/00302).

APPENDIX

Definition of Statistics

a. Eulerian statistics

Time series of Eulerian velocities u_t are measured at different fixed positions (1024 points uniformly and horizontally distributed for each vertical layer). The Eulerian autocorrelation function is calculated as follows (Daoud et al. 2003):

$$R^{\mathrm{E}}(\tau) = \frac{\sum_{t=1}^{N-j} [(u_t - \overline{u}_t)(u_{t+j} - \overline{u}_{t+j})]}{\left[\sum_{t=1}^{N-j} (u_t - \overline{u}_t)^2\right]^{1/2} \left[\sum_{t=1}^{N-j} (u_{t+j} - \overline{u}_{t+j})^2\right]^{1/2}}, \tag{A1}$$

where $\tau = j\Delta t$ is the time lag, and N is the number of time steps Δt. The mean velocities are defined according to

$$\overline{u}_t = \frac{\sum_{t'=1}^{N-j} u_{t'}}{N-j} \quad \text{and} \tag{A2}$$

$$\overline{u}_{t+j} = \frac{\sum_{t'=1}^{N-j} u_{t'+j}}{N-j} = \frac{\sum_{t'=j+1}^{N} u_{t'}}{N-j}. \tag{A3}$$

The autocorrelation is then spatially averaged over all the fixed measurement positions. Spatial autocorrelation is calculated from the velocities u_i measured at different positions along the wind direction (recorded every 10 min) as follows:

$$R^{\mathrm{E}}(r) = \frac{\sum_{i=1}^{N-j} [(u_i - \overline{u}_i)(u_{i+j} - \overline{u}_{i+j})]}{\left[\sum_{i=1}^{N-j} (u_i - \overline{u}_i)^2\right]^{1/2}\left[\sum_{i=1}^{N-j} (u_{i+j} - \overline{u}_{i+j})^2\right]^{1/2}}, \tag{A4}$$

where $r = j\Delta x$ is the space lag, and Δx is the grid size. Autocorrelations calculated according to (A4) have been subsequently averaged over all of the parallel lines and over time.

b. Lagrangian statistics

In the Lagrangian framework, the autocorrelation function is calculated using the particle velocities $u^i(t)$ derived according to (10). At each time $t_0 + \tau$ (where t_0 is the release time and τ is the time lag), the Lagrangian autocorrelation $R^{\mathrm{L}}(\tau)$ is calculated following Wang et al. (1995) as

$$R^{\mathrm{L}}(\tau) = \frac{\langle [u^i(t_0) - \langle u^i(t_0)\rangle][u^i(t_0+\tau) - \langle u^i(t_0+\tau)\rangle]\rangle}{\langle [u^i(t_0) - \langle u^i(t_0)\rangle]^2\rangle^{1/2}\langle [u^i(t_0+\tau) - \langle u^i(t_0+\tau)\rangle]^2\rangle^{1/2}}, \tag{A5}$$

where the average (indicated by $\langle\ \rangle$) is made over all the particles released at the same height.

REFERENCES

Angell, J. K., 1964: Measurements of Lagrangian and Eulerian properties of turbulence at a height of 2500 ft. *Quart. J. Roy. Meteor. Soc.,* **90,** 57–71.

Batchelor, G. K., 1949: Diffusion in a field of homogeneous turbulence. *Aust. J. Sci. Res.,* **2,** 437–450.

Blackadar, A. K., 1998: *Turbulence and Diffusion in the Atmosphere.* Springer, 185 pp.

Briggs, G. A., 1993: Plume dispersion in the convective boundary layer. Part II: Analysis of CONDORS field experiment data. *J. Appl. Meteor.,* **32,** 1388–1425.

Carruthers, D. J., and J. C. Hunt, 1986: Velocity fluctuations near an interface between a turbulent region and a stably stratified layer. *J. Fluid Mech.,* **165,** 475–501.

Caughey, S. J., 1982: Observed characteristics of the atmospheric boundary layer. *Atmospheric Turbulence and Air Pollution Modelling,* F. T. M. Nieuwstadt and H. van Dop, Eds., Reidel, 107–158.

——, and S. G. Palmer, 1979: Some aspects of turbulence structure through the depth of the convective boundary layer. *Quart. J. Roy. Meteor. Soc.,* **105,** 811–827.

Corssin, S., 1963: Estimates of the relations between Eulerian and Lagrangian scales in large Reynolds number turbulence. *J. Atmos. Sci.,* **20,** 115–119.

Csanady, G. T., 1973: *Turbulent Diffusion in the Environment.* D. Reidel, 248 pp.

Cuijpers, J. W. M., and P. G. Duynkerke, 1993: Large eddy simulation of trade wind cumulus clouds. *J. Atmos. Sci.,* **50,** 3894–3908.

Daoud, W. Z., J. W. D. Kahl, and J. K. Ghorai, 2003: On the synoptic-scale Lagrangian autocorrelation function. *J. Appl. Meteor.,* **42,** 318–324.

Deardorff, J. W., and G. E. Willis, 1985: Further results from a laboratory model of the convective planetary boundary layer. *Bound.-Layer Meteor.,* **32,** 205–236.

de Baas, A. F., H. van Dop, and F. T. M. Nieuwstadt, 1986: An application of the Langevin equation for inhomogeneous conditions to dispersion in a convective boundary layer. *Quart. J. Roy. Meteor. Soc.,* **112,** 165–180.

Degrazia, G., D. Anfossi, H. F. D. C. Velho, and E. Ferrero, 1998: A Lagrangian decorrelation time scale in the convective boundary layer. *Bound.-Layer Meteor.,* **86,** 525–534.

Dosio, A., J. Vilà-Guerau de Arellano, A. A. M. Holtslag, and P. J. H. Builtjes, 2003: Dispersion of a passive tracer in buoyancy- and shear-driven boundary layers. *J. Appl. Meteor.,* **42,** 1116–1130.

Georgopoulos, P. G., and J. H. Seinfeld, 1988: Estimate of relative dispersion parameters from atmospheric turbulence spectra. *Atmos. Environ.,* **22,** 31–41.

Gifford, F. A., 1955: A simultaneous Lagrangian-Eulerian turbulence experiment. *Mon. Wea. Rev.,* **83,** 293–301.

——, 1982: Horizontal diffusion in the atmosphere: A Lagrangian-dynamical theory. *Atmos. Environ.,* **16,** 505–512.

——, 1987: The time-scale of atmospheric diffusion considered in relation to the universal diffusion function f_1. *Atmos. Environ.,* **21,** 1315–1320.

Gopalakrishnan, S. G., and R. Avissar, 2000: An LES study of the impacts of land surface heterogeneity on dispersion in the convective boundary layer. *J. Atmos. Sci.,* **57,** 352–371.

Graf, J., and U. Schumann, 1992: Simulation of the convective boundary layer in comparison to aircraft measurements. *Air Pollution Modelling and Its Application, IX,* H. van Dop and G. Kallos, Eds., Plenum Press, 587–593.

Hanna, S. R., 1981: Lagrangian and Eulerian time-scale relations in the daytime boundary layer. *J. Appl. Meteor.,* **20,** 242–249.

Henn, D. S., and R. I. Sykes, 1992: Large eddy simulation of dispersion in the convective boundary layer. *Atmos. Environ.,* **26A,** 3145–3159.

Hinze, O., 1975: *Turbulence.* McGraw-Hill, 790 pp.

Holtslag, A. A. M., and F. T. M. Nieuwstadt, 1986: Scaling the atmospheric boundary layer. *Bound.-Layer Meteor.,* **36,** 201–209.

Kaiser, R., and E. Fedorovich, 1998: Turbulence spectra and dissipation rates in a wind tunnel model of the atmospheric convective boundary layer. *J. Atmos. Sci.,* **55,** 580–594.

Khanna, S., and J. B. Brasseur, 1998: Three-dimensional buoyancy- and shear-induced local structure of the atmospheric boundary layer. *J. Atmos. Sci.,* **55,** 710–743.

Lamb, R. G., 1978: A numerical simulation of dispersion from an elevated point source in the convective planetary boundary layer. *Atmos. Environ.,* **12,** 1297–1304.

——, 1982: Diffusion in the convective boundary layer. *Atmospheric Turbulence and Air Pollution Modelling,* F. T. M. Nieuwstadt and H. van Dop, Eds., Reidel, 159–229.

Lenschow, D. H., and B. B. Stankov, 1986: Length scales in the boundary layer. *J. Atmos. Sci.,* **43,** 1198–1209.

——, J. C. Wyngaard, and W. T. Pennell, 1980: Mean-field and second-moment budgets in a baroclinic, convective boundary layer. *J. Atmos. Sci.,* **37,** 1313–1326.

Mason, P. J., 1989: Large-eddy simulation of the convective boundary layer. *J. Atmos. Sci.,* **46,** 1492–1516.

——, 1992: Large-eddy simulation of dispersion in convective boundary layer with wind shear. *Atmos. Environ.,* **26A,** 1561–1571.

Moeng, C. H., and R. Rotunno, 1990: Vertical-velocity skewness in the buoyancy-driven boundary layer. *J. Atmos. Sci.,* **47,** 1149–1162.

Nieuwstadt, F. T. M., P. J. Mason, C. H. Moeng, and U. Schumann, 1991: Large-eddy simulation of the convective boundary layer: A comparison of four computer codes. *Proc. Eighth Symp. on Turbulent Shear Flows*, Munich, Germany, 343–367.

Ott, S., and J. Mann, 2000: An experimental investigation of the relative diffusion of particle pairs in three-dimensional turbulent flow. *J. Fluid Mech.,* **422,** 207–223.

Pasquill, F., 1974: *Atmospheric Diffusion.* Ellis Horwood Limited, 429 pp.

Phillips, P., and H. A. Panofsky, 1982: A re-examination of lateral dispersion from continuous sources. *Atmos. Environ.,* **16,** 1851–1859.

Sato, Y., and K. Yamamoto, 1987: Lagrangian measurements of fluid-particle motion in an isotropic turbulent field. *J. Fluid Mech.,* **175,** 183–199.

Schmidt, H., and U. Schumann, 1989: Coherent structure of the convective boundary layer derived from large-eddy simulations. *J. Fluid Mech.,* **200,** 511–562.

Siebesma, A. P., and J. W. M. Cuijpers, 1995: Evaluation of parametric assumptions for shallow cumulus convection. *J. Atmos. Sci.,* **52,** 650–666.

Squires, K. D., and J. K. Eaton, 1991: Lagrangian and Eulerian statistics obtained from direct numerical simulation of homogeneous turbulence. *Phys. Fluids,* **3A,** 130–143.

Taylor, G. I., 1921: Diffusion by continuous movements. *Proc. Roy. Soc. London,* **A20,** 196–211.

Tennekes, H., and J. L. Lumley, 1972: *A First Course in Turbulence.* MIT Press, 300 pp.

Thomson, D. J., 1987: Criteria for the selection of stochastic models of particle trajectories in turbulent flows. *J. Fluid Mech.,* **180,** 529–556.

Uliasz, M., and Z. Sorbjan, 1999: Lagrangian statistics in atmospheric boundary layer derived from LES. Preprints, *13th Symp. on Boundary Layers and Turbulence,* Dallas, TX, Amer. Meteor. Soc., P2A.6.

Voth, G. A., K. Satyanarayan, and E. Bodenschatz, 1998: Lagrangian acceleration measurements at large Reynolds numbers. *Phys. Fluids,* **10A,** 2268–2280.

Vreugdenhil, C. B., and B. Koren, Eds., 1993: *Numerical Methods for Advection-Diffusion Problems.* Vol. 45, Vieweg, 373 pp.

Wandel, C. F., and O. Kofoed-Hansen, 1962: On the Eulerian-Lagrangian transform in the statistical theory of turbulence. *J. Geophys. Res.,* **67,** 3089–3093.

Wang, Q., K. D. Squires, and X. Wu, 1995: Lagrangian statistics in turbulent channel flow. *Atmos. Environ.,* **29,** 2417–2427.

Weil, J. C., W. Synder, R. E. L. Jr., and M. S. Shipman, 2002: Experiments on buoyant plume dispersion in a laboratory convection tank. *Bound.-Layer Meteor.,* **102,** 367–414.

——, P. Sullivan, and C. H. Moeng, 2004: The use of large-eddy simulations in Lagrangian particle dispersion models. *J. Atmos. Sci.,* **61,** 2877–2887.

Willis, G. E., and J. W. Deardorff, 1974: A laboratory model for the unstable boundary layer. *J. Atmos. Sci.,* **31,** 1297–1307.

——, and ——, 1976: A laboratory model of diffusion into the convective planetary boundary layer. *Quart. J. Roy. Meteor. Soc.,* **102,** 427–445.

——, and ——, 1981: A laboratory study of dispersion from a source in the middle of the convectively mixed layer. *Atmos. Environ.,* **15,** 109–117.

Wyngaard, J. C., and J. C. Weil, 1991: Transport asymmetry in skewed turbulence. *Phys. Fluids,* **3A,** 155–162.

Yeung, P. K., 2002: Lagrangian investigation of turbulence. *Annu. Rev. Fluid Mech.,* **34,** 115–142.

——, and S. B. Pope, 1989: Lagrangian statistics from direct numerical simulations of isotropic turbulence. *J. Fluid Mech.,* **207,** 531–586.